Astron. Astrophys. 348, 1005–1011 (1999)

ASTRONOMY AND ASTROPHYSICS

Fourier and wavelet analysis of type 42 SER and 41 F solar radio bursts

H. Mészárosová, K. Jiřička, and M. Karlický

Astronomical Institute of the Academy of Sciences of the Czech Republic, CZ-25165 Ondřejov (radio@asu.cas.cz)

Received 2 February 1999 / Accepted 17 June 1999

Abstract. 19 radio bursts (0.01 s time resolution) classified as 42 SER and 41 F types were selected from observations made by the Ondřejov 3 GHz radiometer during 1990–1998. On the 2–4 GHz dynamic radio spectrum in most cases these bursts were identified as decimetric DCIM and in the metric range were accompanied by type III radio bursts indicating the plasma emission origin of these bursts. This set of 3 GHz bursts was analyzed by both the Fourier and the wavelet transform methods searching for characteristic periodicities. Statistical parameters of selected bursts were very similar and almost no difference between 42 SER and 41 F was found. The analysis of the 42 SER and 41 F radio bursts on 3 GHz shows that the number of periods is increasing with decreasing periods, forming a power-law distribution. The dominant periods of the 3 GHz radiation are discussed in the framework of the recent RLC-circuit model with current-carrying magnetic loops. On the basis of this interpretation the electric current densities in the magnetic loops were estimated in the 0.01–0.1 A m^{-2} range.

Key words: acceleration of particles – methods: data analysis – Sun: activity – Sun: flares – Sun: magnetic fields – Sun: radio radiation

1. Introduction

The radio emission of solar flares can be divided roughly into two part: a) mm-cm range component generated by the gyrosynchrotron emission mechanism, and b) dm-m range component having its origin in the plasma emission processes of anisotropic superthermal particles (Krüger 1979). While the component generated by the gyrosynchrotron mechanism is broadband and relatively smooth, the bursts generated by the plasma emission mechanisms are characterized by narrow bandwidths, fine structures and rapid time variations (Bastian et al. 1998). The boundary between a dominance of both components is not fixed, it differs for different solar flares. Our radiospectrographic observations show that this border is in most cases in the 1–4 GHz range. But there are cases when bursts with fast variations and fine structures were observed on still higher frequencies (Kaufmann 1978; Allaart et al. 1990; Raulin et al. 1998; Zodi Vaz et al. 1987; Kaufmann et al. 1980; Butz et al. 1976). Thus, the 3 GHz observations in some flares are low frequency parts of the gyro-emission component, and in others the high frequency part of the plasma-emission one. But using some criteria as e.g. rapid variations, the narrow bandwidth and fine structure on the dynamic spectrum the set of 3 GHz bursts with dominating plasma-emission components can be selected.

The statistical analyses of radio bursts show different time scales in ranges from milliseconds up to tens of minutes (Dröge 1976, 1977; Slottje 1978; Fu Qi-jun et al. 1987; Benz & Aschwanden 1991; Isliker 1992; Barrow et al. 1994; Krüger et al. 1994). This broad range of periods is difficult to explain by a single physical process, therefore for different period ranges different underlying physical processes were suggested (Krüger et al. 1994; Zaitsev et al. 1998).

On the other hand, modern statistical methods show that solar radio bursts are superpositions of transient phenomena, i.e. the underlying physical processes are non-stationary (Isliker & Kurths 1993). Therefore, the multiresolution analysis (MRA) based on the wavelet transform is used (Schwarz et al. 1998). While the classical Fast Fourier Transform (FFT) gives us information about global properties for the whole bursts interval, the MRA yields the local decomposition of characteristic time scales at specific times. Furthermore, the statistical methods for nonlinear dynamical system reveal the presence of the $1/f^{\gamma}$ component in the power spectrum of the 2.5 and 2.85 GHz radio bursts (Ryabov et al. 1998).

In comparison with the classical Fourier approach where periods and periodic processes are searched for, most modern methods show results which are usually without any time structure. We think that some part of this difference is caused by the fact that the spectral resolution of the FFT method is usually higher than that of the wavelet analysis. Therefore, in this paper both these methods (FFT and MRA) are used and the results compared.

Generally, on radio event records individual peaks are superimposed on highly variable "background" radio emission and this makes the analysis of these bursts very complicated. To reduce this problem, we selected such radio events in which for specific time scales the individual burst peaks start and end on some more or less constant radio flux level. (Clearly, with the increase of the time resolution the character of these bursts can

Send offprint requests to: H. Mészárosová

Table 1. List of analyzed radio events.

Event No.	Date [dd-mm-yyyy]	Type	Start time [UT]	Interval [min]	Spectral type m range	Spectral type dm range
1	12-03-1991	41 F	13:59:10	2	III G	–
2	13-03-1991	42 SER	08:02:30	1	III GG	–
3	16-04-1991	41 F	11:41:20	2	–	–
4	16-04-1991	41 F	11:49:00	2	–	–
5	29-05-1991	41 F	09:31:00	2	–	DCIM G
6	12-06-1991	42 SER	07:06:00	2	III G	DCIM G
7	14-07-1991	41 F	06:36:00	2	III G	–
8	06-11-1991	41 F	11:24:30	2	III GG	DCIM GG
9	16-02-1992	41 F	09:20:50	2	–	–
10	16-02-1992	41 F	09:28:10	2	–	–
11	24-10-1992	42 SER	10:37:40	1	–	–
12	07-04-1993	42 SER	13:17:10	6	–	–
13	07-04-1993	42 SER	13:39:20	4	–	–
14	19-10-1993	41 F	08:45:40	2	–	–
15	06-01-1994	41 F	10:34:20	2	–	–
16	09-06-1996	41 F	09:06:40	1	–	DCIM G
17	28-08-1996	41 F	08:03:00	2	III G	DCIM G
18	15-04-1998	41 F	07:59:00	3	III GG	DCIM GG
19	30-07-1998	41 F	08:04:55	1	III N	DCIM GG

change but in a detailed view again the peaks superposed on the variable "background" emission can be seen). According to a coding of the Solar Geophysical Data (SGD) journal these types of bursts are designated as type 42 SER and 41 F. On the radio spectrum these bursts were for some cases identified as DCIM bursts indicating the plasma emission origin of the selected bursts.

The organization of this paper is as follows: We present our data set (Sect. 2) and introduce the FFT and MRA tools of the data analysis (Sect. 3). The obtained results (Sect. 4) are discussed and conclusions drawn (Sect. 5).

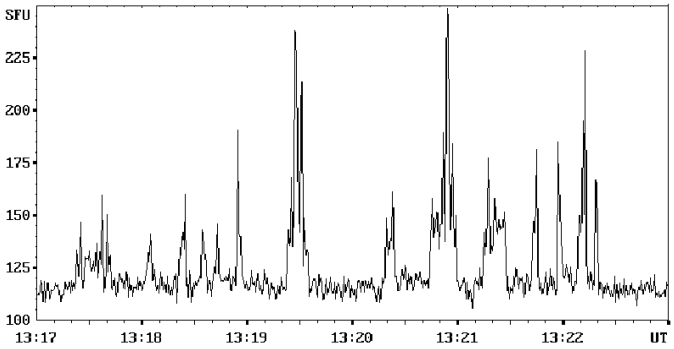

Fig. 1. An example of the type 42 SER burst at 3 GHz (observed on April 07, 1993 at Ondřejov) – no spectrum available

2. The 3 GHz solar radio data

In this paper the decimetric bursts observed at the Astronomical Institute in Ondřejov are analyzed. The Ondřejov RT3 receiver (Jiřička & Snížek 1994) measures solar radio flux at 3.0 GHz with 0.01 s time resolution and the sensitivity of the receiver at this time resolution is of about 4 SFU. The observations are run daily, but only radio events are archived. Since September 1990, when we started archiving data in digital form, over 400 events have been registered.

As mentioned in the Introduction, to reduce the problem with the transient character of the 3.0 GHz bursts, we selected only such radio events in which the individual bursts start and end on a more or less constant radio flux level (see e.g. Fig. 1). According to the Solar Geophysical Data (SGD) journal definition such radio bursts are designated as type 42 SER (a series of bursts starting intermittently from a base level with considerable time intervals – see Fig. 1) and type 41 F (a group of minor bursts close to each other – see Fig. 2).

Total number of events selected is 19 (see Table 1). On the radio spectrum, in the decimetric frequency range, these bursts were identified as a group of DCIM radio bursts (see spectrum in Fig. 2), where the DCIM means a complex, highly structured emission between 300 and 3000 MHz (SGD definition). On the other hand, in the metric range, these bursts were often accompanied by a group of type III radio bursts.

3. Statistical analysis methods

The main purpose of the data processing was to determine the periodicities in the observed radio fluxes by the Fourier method, to estimate the likelihood of the results and to compare these results with the wavelet data transform information.

3.1. The fast Fourier transform (FFT) method

Since we are trying to obtain power spectra with minimal distortion the following two operations on input time series (Karlický 1977) were used:

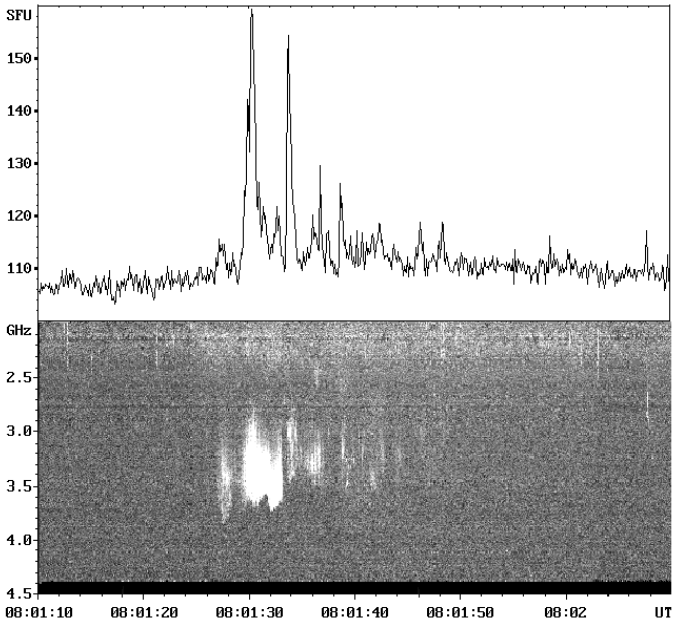

Fig. 2. An example of the type 41 F burst at 3 GHz and the corresponding 2.0 - 4.5 GHz radio spectrum (observed on April 15, 1998 at Ondřejov)

a/ The operation MEAN transforms the series of values into series with zero mean value.
b/ The operation WIND modifies the beginning and ending values of the series by multiplying them with a weight function - the window. In our case we used the so-called cosine bell window defined as

$$w_x = \begin{cases} \frac{1}{2}(1-\cos\pi\frac{x}{fN}) & x \in \langle 0, fN\rangle \\ 1 & \text{for } x \in \langle fN, N-fN\rangle \\ \frac{1}{2}(1-\cos\pi\frac{N-x}{fN}) & x \in \langle N-fN, N\rangle \end{cases} \quad (1)$$

where N is the length of the series and f is the portion of the length of the series shaped by the cosine bell window (in our case f was taken to equal 0.1).

Periodograms (power spectra) are obtained by applying the POW procedure (Press et al. 1986) on the time series:

If we form a time series c_x by taking N equidistant samples of the function c(t), apply the procedure MEAN and use the FFT to compute its discrete Fourier transform

$$D_k = \sum_{x=0}^{N-1} c_x w_x e^{\frac{2\pi i x k}{N}} \qquad for \qquad k = 0, ..., N-1 \quad (2)$$

then the periodogram estimate of the windowed time series spectrum is defined at $N/2+1$ frequencies f_k as

$$P(f_k) = \begin{cases} \frac{1}{W_s}|D_k|^2 & k = 0 \\ \frac{1}{W_s}(|D_k|^2 + |D_{N-k}|^2) & \text{for } k = 1, ..., \frac{N}{2}-1 \\ \frac{1}{W_s}|D_k|^2 & k = \frac{N}{2} \end{cases} \quad (3)$$

where W_s stands for "window squared and summed"

$$W_s = N\sum_{x=0}^{N} w_x^2, \quad (4)$$

and frequencies f_k are defined as

$$f_k = \frac{k}{N\Delta t} \qquad \text{for} \quad k = 0, 1, ..., \frac{N}{2} \quad (5)$$

where Δt is the time interval between the equidistant samples.

To eliminate the effects of noise and increase the likelihood of found periods, the periodograms are smoothed by the following method (Karlický 1977): if the original series of $N/2+1$ periodogram values is called P and the smoothed one I, then

$$I_k = \begin{cases} k_0 P_k + 2k_1 P_{k+1} & k = 0 \\ k_0 P_k + k_1(P_{k-1} + P_{k+1}) & \text{for } k = 1, ..., \frac{N}{2}-1 \\ k_0 P_k + 2k_1 P_{k-1} & k = \frac{N}{2} \end{cases} \quad (6)$$

with $k_0 = 0.54$ and $k_1 = 0.23$.

If a local maximum in the periodogram indicates presence of a periodicity in the time series, the question arises if this peak is real or if it is just noise. We can never tell for certain, we can just determine the probability of this maximum being real. If this probability exceeds certain value we can consider the periodicity to be likely. In our case, as likely we considered the peaks with probability above 0.75.

The computation of the likelihood P_0 of individual peaks in the smoothed periodogram I is carried out by applying the method described in the paper by Pračka & Karlický (1979):

We consider the individual values of the periodogram as random variables with distribution function

$$\chi^2_\nu(u) = \frac{1}{2\Gamma(\frac{\nu}{2})}(\frac{u}{2})^{\frac{\nu}{2}-1}e^{-\frac{u}{2}} \quad (7)$$

where ν is the number of degrees of freedoms (ν equals 2 for the unsmoothed periodogram and about 5 for the periodogram smoothed by Eq. 6).

Now we must determine the limits of the interval of confidence A and B by numerically solving the system of two equations

$$\int_0^A \chi^2_\nu(u)\,du = \int_B^\infty \chi^2_\nu(u)\,du \quad (8)$$

$$\frac{I_{max}}{B} = \frac{I_{min}}{A} \quad (9)$$

where

I_{max} is the value of the investigated local maximum in the smoothed periodogram and
I_{min} is the value of the local minimum neighbouring on the maximum being investigated.

The probability P_0 of the investigated maximum can then be determined by integrating the distribution function over the interval of confidence

$$P_0 = \int_A^B \chi^2_\nu(u)\,du \quad (10)$$

3.2. The triangle-like wavelet transform (MRA) method

Wavelet multiresolution analysis (MRA)(Bendjoya et al. 1993; Cohen & Kovacevic 1996) is the proper tool to study phenomena with the inhomogeneous scaling behaviour, varying in space

and/or in time. The wavelet analysis allows the local decomposition of time scales in time series of transient nature or non-stationary processes. This is an important extension to Fourier analysis, which is designed to provide the global decomposition of time series with stationary properties.

We use the discrete wavelet algorithm described by Schwarz at al. (1998) and Aschwanden et al. (1998). The wavelet analysis is based on time-limited elements, the wavelets. The wavelet transform of $x(t)$ is a decomposition into a basis of functions $\omega_{a,b}(t)$

$$\omega_{a,b}(t) = |a|^{-\frac{1}{2}}\omega(\frac{t-b}{a}) \tag{11}$$

all derived from a unique function $\omega(t)$, called the "mother wavelet", by translation $b = k\Delta t$ and scaling $a = 2^j$. Several functions have been recommended as wavelets. For our purpose, the simple triangle-like wavelet is appropriate, because its shape fits the time profile of the radio flux quite well (Schwarz et al. 1998).

This method yields consistent values of the spectral index which describes the scalings contained in the time series of unfiltered data. The dynamic decomposition of the power at different time scales T (the scalogram) is best portrayed as a $2^j\Delta t$ versus $k\Delta t$ plot of the wavelet coefficients d_k^j and shows the scaling behaviour of the radio flux $x(t)$ in dependence on the time location $k\Delta t$. Averaging the squares of wavelet coefficients d_k^j over the whole studied time interval $N\Delta t$ we obtain a function of time scale T_j $(= 2^j\Delta t)$, the so called scalegram s

$$s(T_j) = \frac{1}{N}\sum_{k=0}^{N-1}|d_k^j|^2 \tag{12}$$

which represents the MRA analog to the FTT power spectrum density (periodogram).

With increasing frequency and decreasing power density it is difficult to determine, if the structures are real or just artifacts from noise, digital sampling, etc. To establish the sensitivity we use the method suggested by Bendjoya et al. (1993): we calculate scalegrams of quiet sun prior to the studied event $s_q(T_j)$ and compare them with the scalegram $s(T_j)$ of the studied event. As significant we then take only those values of time scales, which exceed the quiet sun values by a certain factor $k\sigma$ (which corresponds to S/N ratio $> k$). Thus we determine the minimum value of time scale T_{min} for which holds

$$\frac{s(T)}{s_q(T)} \geq k \quad \text{for} \quad T \geq T_{min} \tag{13}$$

and we consider all time scales above T_{min} as probable. With increasing factor k the likelihood of time scales is increasing but their number is diminishing. As a compromise, Bendjoya et al. (1993) suggest as optimal minimum value $k = 1.6$ (likelihood 95%).

4. Results

The analysis of all events from Table 1 was carried out by using the above described Fourier method and the method of estimating the likelihood of peaks in periodograms. With respect the 10 ms time resolution of the receiver and to reduce the effects of sampling, we considered only periodicities larger then 20 sampling points, i.e. periodicities above 200 ms. To reduce the effects of noise we established by help of the MRA the 1.6σ limits T_{min} for all studied bursts (see Table 2 and example of determining the T_{min} limit for event No. 9 in Fig. 6) and for the analysis we consider only those periods P which exceed both the T_{min} limits and the 200 ms limit

$$P_{min} = MAX(T_{min}, 0.2) \tag{14}$$

Table 2. Summary of $T_{min}(1.6\sigma)$, P_{min} and periodicities with likelihood over 75% for events from Table 1.

Event No.	T_{min} [s]	P_{min} [s]	Periods $>$ 3s [s]	Periods $<$ 3s [number]
1	1.30	1.30	24.0	3
2	0.07	0.20	–	8
3	0.20	0.20	–	15
4	0.30	0.30	5.2	10
5	0.40	0.40	24.0	7
6	0.09	0.20	3.6, 6.0	13
7	1.30	1.30	3.9, 5.2	1
8	0.80	0.80	40.0	4
9	0.04	0.20	10.0	9
10	0.20	0.20	3.2, 5.0, 10.0	17
11	0.10	0.20	3.0, 15.0	5
12	0.16	0.20	3.1, 6.7, 10.9	32
13	0.30	0.30	3.2, 10.0	11
14	0.50	0.50	6.3, 20.0	3
15	2.50	2.50	–	1
16	0.70	0.70	–	1
17	0.10	0.20	7.5	18
18	0.06	0.20	3.2, 5.7	30
19	0.30	0.30	20.0	9

4.1. Results of the FFT

From the point of view of statistical likelihood as likely we considered the peaks with probability above 0.75. For individual events we found dominant periodicities in the 40–3 s interval (see Table 2). Furthermore, for all events we found number of periods in the 3–0.02 s interval. As example, in the Fig. 3 you can see a part of the power spectrum (periodogram) and in the Table 3 you can find list of periods with corresponding probabilities found for the No. 9 (February 16, 1992) event.

For purpose of comparison, we calculated FFT power spectra densities of quiet Sun for 60 s time intervals prior to the analyzed events. In no case the likelihood of periodogram peaks reached the 75% limit.

Since all the studied bursts are of the similar type (classification based on the single-frequency and spectral records), we summarized the periods found in all analyzed events in one period distribution graph shown in Fig. 4. For periods longer than 3 seconds we can see isolated periods. On the other hand, below the 3 s limit towards smaller periods the number of periods is increasing with decreasing periods, forming a power-law distri-

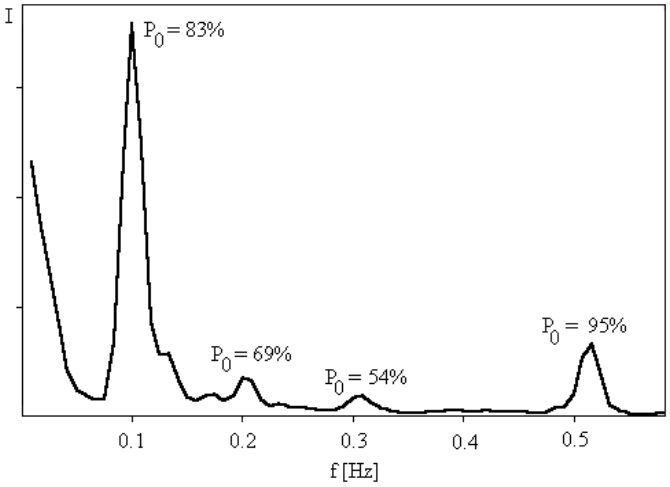

Fig. 3. Part of the power spectrum (periodogram) of the event No. 9 (See Fig. 5).

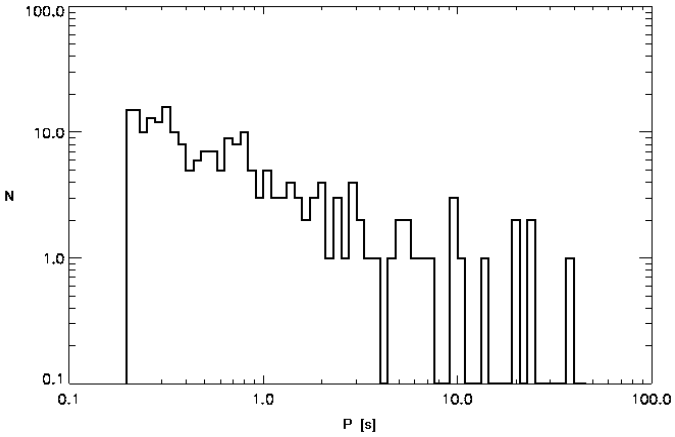

Fig. 4. The distribution of periods with likelihood above 75% and above P_{min} for all the events from Table 1.

Table 3. Periods and their probabilities for the event No. 9 (February 16, 1992 at 09:20:50 UT).

Period $P[s]$	Probability $P_0[\%]$
10.000	83
1.935	95
1.395	89
0.536	91
0.480	83
0.354	81
0.314	83
0.264	93
0.235	86
0.203	83

bution. This plot represents a summary of periodic components found for all studied events (compare with Table 2).

4.2. Results of the MRA

We applied the MRA on the dm-radio time profiles $x(t)$ of solar burst events listed in Table 1. Using the MRA we observed that the wavelet coefficients d_k^j reflect the burst-like behaviour of the radio flux quite well.

We plotted the scalograms as the logarithm of the normalized wavelet coefficients $log_2 d_k^j$. Different values of the coefficients (amplitudes) are displayed by different levels of grey.

As an example, we show in the upper part of Fig. 5 the radio flux time profile of the event No. 9 (observed on February 16, 1992 in Ondřejov) with corresponding scalogram with 12 time scales between 0.02 s and 40.96 s. This profile $x(t)$ has time resolution Δt = 0.01 s and a length of N = 6000 data points, i.e. 60 s.

We also found fine structures in individual bursts for all analyzed events. As an example, in the lower part of Fig. 5 you can see the blown-up detail of the event No. 9 with corresponding scalogram. This profile $x(t)$ has the same time resolution of Δt = 0.01 s and a length of N = 1100 data points i.e. 11 s.

Results of the MRA agree quite well with results of the FFT. The wavelet transforms, calculated for all events from Table 1, indicate that a broad range of time scales from 40 s to 0.2 s is involved. But, due to lower spectral resolution of MRA comparing with FFT, the "single" periods cannot be recognized. On the other hand, the sequences of bright patterns in the scalograms (see Fig. 5) give us an idea of the dominant scales at different times during the bursts.

5. Discussions and conclusions

No substantial statistical differences between 42 SER and 41 F type bursts or between individual events were found by this statistical analysis. It enables us to assume that the selected bursts are of the similar physical origin. From the limited spectral information we have at disposal it looks as probable that the bursts under study belong to the high-frequency part of the dm-m flare radio component generated by the plasma emission mechanism.

Using the Fourier and wavelet analysis, in all studied 42 SER and 41 F radio bursts it was found that while the dominant periods are present in the lower period range the number of recognized periods with probability over 75% increases with decreasing period forming a power-law distribution which may be equivalent to that found by Ryabov et al. (1998). For interpretation of dominant periods several models were suggested in the literature (for review of these models – see Krüger et al. 1994). Recently, a new improved RCL-circuit model of Zaitsev et al. (1998) was published. In the following we apply this model for the interpretation of dominant detected periods.

According to Zaitsev et al. (1998) the periods in the radio emission can be explained by those in the current loop. These current loops and corresponding magnetic field can oscillate with periods P

$$P = \frac{2\pi}{c}(LC)^{1/2} \qquad (15)$$

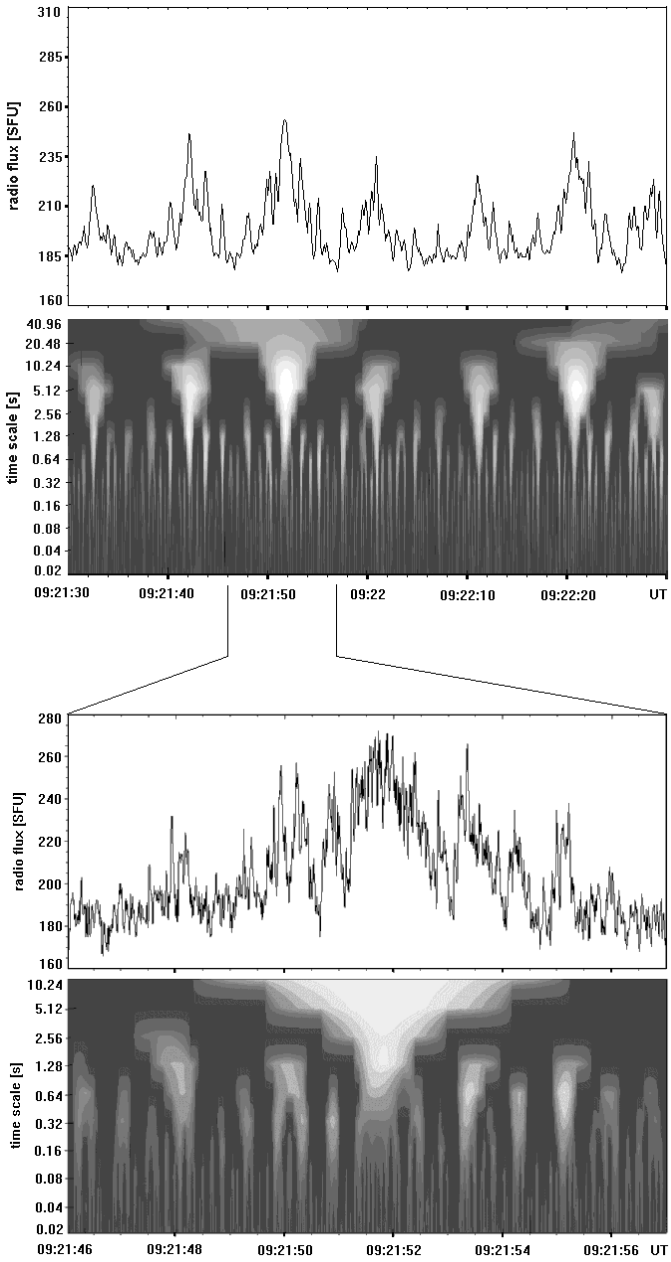

Fig. 5. Radio flux time profile at 3 GHz of the event No. 9 of February 16, 1992 (Ondřejov) and the corresponding scalogram (upper part) and a blown-up detail of the same (lower part).The white patterns represent the dominant time scales.

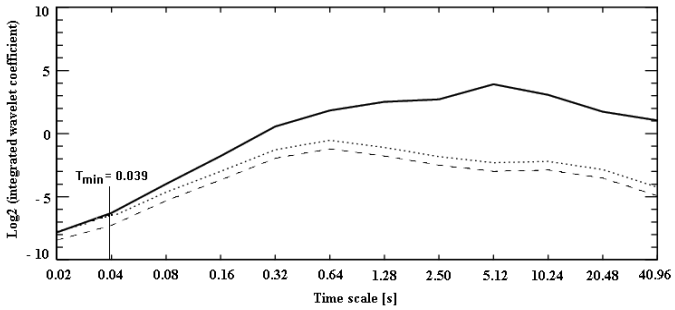

Fig. 6. Scalegram of event No.9 (solid line), scalegram of the quiet sun prior to the event (dashed line) and the 1.6σ scalegram of the quiet sun (dotted line)

where c is the speed of light, and C and L are the circuit capacitance and inductance, which can be expressed as

$$C = \frac{c^4 \rho S^2}{2\pi l I^2} \tag{16}$$

$$L = 4l\left(\ln\frac{8l}{(\pi S)^{1/2}} - \frac{7}{4}\right) \tag{17}$$

where ρ, l, and S are the plasma density, length, and cross-sectional area of the coronal part of a loop, respectively, and I is the electric current along the loop axis. In the paper of Zaitsev et al. (1998) the periods were used for the determination of the total flare current. But in our case, because there is no information about the current loop geometry, we used these formulas for the current density estimation. It is important to emphasize that in our case the product LC and also the period do not depend on the length of the current loop. It means that the formula for the oscillation period can be considered not only for the full circuit oscillations but also for localized current loop parts. Moreover, the ratio I/S expresses the electric current density. Thus, for the period of oscillations in the current loop and also in radio emission we can write

$$P \simeq \frac{3\ 10^4}{j}. \tag{18}$$

Now from periods found by the Fourier analysis and using SI unit system, we can determine electric current densities in the activated current filament as:

$$j \simeq \frac{1}{10\ P} \quad [Am^{-2}; s]. \tag{19}$$

Several periods for one event we interpret as several separate or co-spatial current filaments with appropriate current densities. Thus, for the dominant periods of 10, 5, 3, and 1 s, the electric current densities of 0.01, 0.02, 0.033, and 0.1 Am^{-2}, respectively, were estimated. For comparison, the current densities measured at the photospheric layers by full-vector magnetographs are in the range 10^{-3} – 10^{-2} Am^{-2} (Hagyard 1988). The estimated values of electric current densities in expected current loops are higher which is probably due to the compression of the activated current filaments close to the 42 SER and 41 F radio sources. The magnetic field reconnection, releasing the energy for radio bursts too, can cause this compression.

Acknowledgements. We acknowledge the support from the key project K1-043-601, and the grant A3003707 of the Academy of Sciences of the Czech Republic. We thank Drs. U. Schwarz and J. Kurths for help with the wavelet analysis methods and the unknown referee for critical comments which helped to improve the paper.

References

Allaart M.A.F., van Nieuwkoop J., Slottje C., Sondaar L.H., 1990, Solar Phys. 130, 183

Aschwanden M.J., Kliem B., Schwarz U., et al., 1998, ApJ 506, 1
Barrow C.H., Zarka P., Aubier M.G., 1994, A&A 286, 597
Bastian T.S., Benz A.O., Gary D.E., 1998, ARA&A 36, 131
Bendjoya P., Petit J.M., Spahn F., 1993, Icarus 105, 385
Benz A.O., Aschwanden M.J., 1991, In: Lecture Notes in Physics, IAU Coll., p. 133
Butz M., Hirth W., Fürst E., Hearth W., 1976, Kleinheubacher Ber. 19, 345
Cohen A., Kovacevic J., 1996, Proc. IEEE 84, 514
Dröge F., 1976, Kleinheubacher Ber. 19,351
Dröge F., 1977, A&A 57, 285
Fu Qi-jun, Jin Sheng-zhen, Zhao Ren-yang, et al., 1987, In: Dennis B.R., Orwig L.E., Kiplinger A.L. (eds.) Rapid Fluctuations in Solar Flares. NASA Conf. Publ. NASA CP 2449, 237
Hagyard M.J., 1988, Solar Phys. 115, 107
Isliker H., 1992, Solar Phys. 141, 325
Isliker H., Kurths J., 1993, Int. J. Bifurcation and Chaos 3, 1573
Jiřička K., Snížek V., 1994, Solar Radio Burst Observations at 10 cm. Publications of the Astronomical Institute of the Academy of Sciences of the Czech Republic No. 83
Karlický M., 1977, Bull. Astron. Inst. Czech. 28, 200
Kaufmann P., 1978, Solar Phys. 60, 367
Kaufmann P., Strauss F.M., Opher R., Laporte C., 1980, A&A 87, 58
Krüger A., 1979, Introduction to Solar Radio Astronomy and Radio Physics. D. Reidel Publ. Comp., Dordrecht, Holland
Krüger A., Kliem B., Hildebrandt J., Zaitsev V.V., 1994, ApJS 90, 683
Pračka M., Karlický M., 1979, Bull. Astron. Inst. Czech. 30, 257
Press W.H., Flannery B. P., Teukolsky S.A., Vetterling W.T., 1986, Numerical Recipes. Cambridge University Press
Raulin J.P., Kaufmann P., Olivieri R., et al., 1998, AJ 498, L173
Ryabov V.B., Stepanov A.V., Usik P.V., et al., 1998, A&A 324, 750
Schwarz U., Kurths J., Kliem B., Krüger A., Urpo S., 1998, A&AS 127, 309
Slottje C., 1978, Nat 275, 520
Zaitsev V.V., Stepanov A.V., Urpo S., Pohjolainen S., 1998, A&A 337, 887
Zodi Vaz A.M., Kaufmann P., Correia E., et al., 1987, In: Dennis B.R., Orwig L.E., Kiplinger A.L. (eds.) Rapid Fluctuations in Solar Flares. NASA Conf. Publ. NASA CP 2449, 237